

Coulomb-exchange effects in nanowires with spin splitting due to a radial electric field

F. S. Gray, T. Kernreiter, M. Governale,* and U. Zülicke†

*School of Chemical and Physical Sciences and MacDiarmid Institute for Advanced Materials and Nanotechnology,
Victoria University of Wellington, PO Box 600, Wellington 6140, New Zealand*

(Dated: March 2, 2024)

We present a theoretical study of Coulomb exchange interaction for electrons confined in a cylindrical quantum wire and subject to a Rashba-type spin-orbit coupling with radial electric field. The effect of spin splitting on the single-particle band dispersions, the quasiparticle effective mass, and the system's total exchange energy per particle are discussed. Exchange interaction generally suppresses the quasiparticle effective mass in the lowest nanowire subband, and a finite spin splitting is found to significantly increase the magnitude of the quasiparticle-mass suppression (by upto 15% in the experimentally relevant parameter regime). In contrast, spin-orbit coupling causes a modest (1%-level) reduction of the magnitude of the exchange energy per particle. Our results shed new light on the interplay of spin-orbit coupling and Coulomb interaction in quantum-confined systems, including those that are expected to host exotic quasiparticle excitations.

PACS numbers: 81.07.Gf, 71.70.Ej, 71.70.Gm, 81.05.Ea

I. INTRODUCTION

The dimensionality of a many-particle system is a crucial determinant for how importantly interaction effects can shape its physical properties. Generally, three-dimensional (3D) bulk conductors are less drastically affected by the Coulomb interaction between charge carriers than lower-dimensional, quantum-confined structures such as quasi-2D quantum wells and quasi-1D quantum (nano-)wires.¹ This is essentially due to phase-space restrictions arising from free motion being only possible in fewer than three spatial directions. Furthermore, the exact structure of transverse bound-state wave functions shapes the density distribution of the confined charge carriers and, thus, turns out to critically influence Coulombic effects in quantum wells² and wires.³ Here we explore how another aspect of quantum-confined states, namely their intrinsic spinor structure, modifies the effect of the Coulomb interaction in nanostructured systems.

Most low-dimensional conductors are fabricated from semiconductor materials where the coupling between the spin degree of charge carriers and their orbital motion is often quite strong.⁴ As a result, quantum confinement can significantly affect spin-related properties.⁵ Such effects are particularly pronounced for valence-band states (i.e., *holes*) because of their peculiar spin-3/2 character.^{5,6} In contrast, conduction-band electrons are spin-1/2 particles and generally subject to weaker spin-orbit couplings that are due to the bulk inversion asymmetry in the material's crystallographic unit cell (Dresselhaus⁷ spin splitting) or the structural inversion asymmetry present in a nanostructured systems (Rashba^{8,9} spin splitting). The multitude, and often counter-intuitive nature, of spin-orbit effects in nanostructures has become the focus of recent study, with developing an understanding of the interplay with Coulomb interactions being a key question to be addressed. Bulk-hole systems,^{10–13} quantum-well-confined holes,^{14–18} and 2D electron systems subject to Rashba spin splitting^{16,19–22} have been

considered. The comparatively few studies of Coulomb-interaction effects in spin-orbit-coupled quasi-1D systems^{23–26} have almost exclusively focused on effective Luttinger-liquid descriptions²⁷ and, in particular, did not investigate the effect of Rashba spin splitting on the total exchange energy and exchange-induced quasiparticle-effective-mass renormalization in quantum wires.

In this article, we fill precisely this gap and investigate both the exchange energy and effective-mass renormalization in quantum wires with a Rashba-type spin-orbit coupling. Previous work on the exchange energy of quantum wells revealed that spin-orbit coupling has the opposite effect on interactions in n-type and p-type systems: the exchange energy of a quasi-2D conduction-band electron system is slightly enhanced^{16,21} due to spin-orbit coupling, whereas the exchange energy for quasi-2D holes is suppressed due to confinement-induced valence-band mixing¹⁸ and the heavy-hole-type Rashba spin splitting.¹⁶ The different behavior of confined band electrons and holes warrants more systematic investigation and, as we will see below, considering the quasi-1D case sheds new light on the different ramifications of spin-orbit coupling in interacting systems. Our investigation also reveals that the quasiparticle effective-mass is more strongly suppressed by the exchange interaction in nanowires with spin splitting.

In addition, quantum wires with strong spin-orbit coupling are currently attracting great interest as possible hosts of exotic quasiparticle excitations such as Majorana²⁸ and fractional²⁹ fermions. Clarifying the effect of interactions in such systems is necessary for a complete understanding of experiments aimed at verifying the existence of the unusual quasi-particle excitations.

The remainder of this article is organised as follows. We introduce our theoretical model of a Rashba-spin-split quantum wire in Sec. II and discuss pertinent properties of the single-particle eigenstates. The formalism for calculating the exchange energy for this system is presented in Sec. III, together with the results. Amongst

these is the ability to express functional dependencies of the exchange energy per particle in terms of a universal scaling function, and the enhanced suppression of the density-of-states effective mass. Our findings are summarized, and related to the existing body of knowledge, in Sec. IV. Certain formal details are given in Appendices.

II. THEORETICAL DESCRIPTION OF RASHBA-SPLIT NANOWIRE STATES

In our study, we aim to develop a general understanding of the effect of spin-orbit coupling on exchange-related many-particle corrections in quasi-1D nanowires. Hence, rather than attempting to describe the detailed electron density profile for a specific sample based on a self-consistent Poisson-Schrödinger calculation, we consider a model cylindrical quantum wire with radius R that is defined by a hard-wall potential where a constant radial electric field $\mathcal{E} = \mathcal{E} \hat{\mathbf{r}}$ gives rise to a spin-orbit coupling of the Rashba type. In a real sample, such a radially symmetric field configuration could be generated, e.g., via biasing of an external gate that is wrapped around the wire surface.³⁰ The pragmatic assumption of a constant electric-field magnitude is justified in Appendix A. See especially Fig. 6. For our situation of interest, the noninteracting-electron dynamics in the wire is described by the Hamiltonian $H = H^{(0)} + U(r)$, where

$$U(r) = \begin{cases} 0 & r < R \\ \infty & r \geq R \end{cases}, \quad (1)$$

and $H^{(0)}$ is a Rashba-type^{8,9} single-electron Hamiltonian

$$H^{(0)} = \frac{\mathbf{p}^2}{2m^*} + \frac{\alpha \mathcal{E}}{\hbar} \hat{\mathbf{r}} \cdot (\boldsymbol{\sigma} \times \mathbf{p}) \quad . \quad (2)$$

Here m^* is the band mass of electrons in the semiconductor material making up the nanowire, α is the material-dependent Rashba spin-orbit-coupling constant, and $\boldsymbol{\sigma} = (\sigma_x, \sigma_y, \sigma_z)^T$ denotes the vector of Pauli matrices. We will find the confined-electron states in the nanowire by superimposing solutions of the single-particle Schrödinger equation $H^{(0)} \psi = E \psi$ to satisfy the cylindrical hard-wall boundary condition.

The Hamiltonian (2) can be conveniently expressed in cylindrical coordinates (r, φ, z) as

$$H^{(0)} = -\frac{\hbar^2}{2m^*} \left(\frac{\partial^2}{\partial r^2} + \frac{1}{r} \frac{\partial}{\partial r} + \frac{1}{r^2} \frac{\partial^2}{\partial \varphi^2} + \frac{\partial^2}{\partial z^2} \right) \mathbb{1} + i \alpha \mathcal{E} \left[\sigma_z \frac{1}{r} \frac{\partial}{\partial \varphi} + i (e^{-i\varphi} \sigma_+ - e^{i\varphi} \sigma_-) \frac{\partial}{\partial z} \right], \quad (3)$$

where $\sigma_{\pm} = (\sigma_x \pm i \sigma_y)/2$ are the spin-1/2 ladder operators. The explicit form of (3) motivates a separation *Ansatz* for the eigenstates of $H^{(0)}$:

$$\psi(r, \varphi, z) = \frac{e^{ikz}}{\sqrt{L}} e^{i\nu\varphi} e^{-i\frac{\sigma_z}{2}\varphi} \phi_{\nu,k}(r) \quad , \quad (4)$$

where $\phi_{\nu,k}(r)$ is the radial spinor wave function, $\nu = \pm 1/2, \pm 3/2, \dots$ is an odd half-integer number, k denotes the wave number associated with the free electron motion in the quantum wire, and L is the wire length. The resulting radial Schrödinger equation that determines $\phi_{\nu,k}(r)$ can be written in dimensionless form as $\mathcal{H}_{\nu,\kappa} \chi_{\nu,\kappa}(\varrho) = \varepsilon \chi_{\nu,\kappa}(\varrho)$, with

$$\mathcal{H}_{\nu,\kappa} = - \left(\frac{\partial^2}{\partial \varrho^2} + \frac{1}{\varrho} \frac{\partial}{\partial \varrho} \right) \mathbb{1} + \frac{\hat{m}^2}{\varrho^2} - \tilde{\alpha} \sigma_z \frac{\hat{m}}{\varrho} + \tilde{\alpha} \kappa \sigma_y + \kappa^2 \mathbb{1}, \quad (5)$$

and the definitions $\hat{m} = \nu \mathbb{1} - \frac{1}{2} \sigma_z$, $\varrho = r/R$, $\kappa = kR$, $\varepsilon = E/E_0$ where $E_0 = \hbar^2/(2m^*R^2)$, $\tilde{\alpha} = 2Rm^*\alpha\mathcal{E}/\hbar^2$, and $\phi_{\nu,k}(r) \equiv \chi_{\nu,\kappa}(r/R)/R$.

We employ the subband $\mathbf{k} \cdot \mathbf{p}$ method^{31,32} to find the cylindrical-nanowire eigenstates and single-particle subband-energy dispersions $E_{nk}^{(0)}$. Simultaneous invariance under time reversal ($\sigma_y \mathcal{H}_{-\nu,-\kappa}^* \sigma_y = \mathcal{H}_{\nu,\kappa}$) and spatial inversion ($e^{-i\frac{\pi}{2}\sigma_z} \mathcal{H}_{\nu,-\kappa} e^{i\frac{\pi}{2}\sigma_z} = \mathcal{H}_{\nu,\kappa}$) imply that each subband is (at least) doubly degenerate.³³ The first step is to find the eigenstates that are associated with the subband-edge energies $E_{n0}^{(0)}$. These states are then used as a basis set for expressing the eigenstates at general $k \neq 0$; with expansion coefficients determined from solving a matrix equation that is equivalent to the Schrödinger equation.

The Hamiltonian of Eq. (5) is diagonal when $\kappa = 0$,

$$\mathcal{H}_{\nu,0} = \begin{pmatrix} H_{\nu} & 0 \\ 0 & H_{-\nu} \end{pmatrix}, \quad (6a)$$

$$H_{\nu} = - \left(\frac{\partial^2}{\partial \varrho^2} + \frac{1}{\varrho} \frac{\partial}{\partial \varrho} \right) + \frac{(\nu - \frac{1}{2})^2}{\varrho^2} - \tilde{\alpha} \frac{\nu - \frac{1}{2}}{\varrho}, \quad (6b)$$

hence the subband-edge states are also spin-projection eigenstates of σ_z with eigenvalue $\sigma = \pm 1$. We can therefore write

$$\chi_{\nu,\kappa}(\varrho) = \sum_{n'=1}^{\infty} \left(c_{\nu,\kappa}^{(n'\uparrow)} |\nu, \uparrow, n'\rangle + c_{\nu,\kappa}^{(n'\downarrow)} |\nu, \downarrow, n'\rangle \right), \quad (7a)$$

with the subband-edge basis-state definitions

$$|\nu, \uparrow, n'\rangle = \mathcal{F}_{\nu-\frac{1}{2}}^{(\varepsilon_{\nu,\sigma}^{(n')})}(\varrho) \begin{pmatrix} 1 \\ 0 \end{pmatrix}, \quad (7b)$$

$$|\nu, \downarrow, n'\rangle = \mathcal{F}_{-\nu-\frac{1}{2}}^{(\varepsilon_{\nu,\sigma}^{(n')})}(\varrho) \begin{pmatrix} 0 \\ 1 \end{pmatrix}, \quad (7c)$$

and the functions $\mathcal{F}_{\sigma\nu-\frac{1}{2}}^{(\varepsilon_{\nu,\sigma}^{(n')})}(\varrho)$ being solutions of the radial-confinement problem defined by the Hamiltonian $H_{\sigma\nu} + U(\varrho R)/E_0$ with corresponding dimensionless eigenenergies $\varepsilon_{\nu,\sigma}^{(n')}$. We number the subband-edge states for fixed ν and σ in ascending order of energy, that is $\varepsilon_{\nu,\sigma}^{(n')} > \varepsilon_{\nu,\sigma}^{(n'')}$ when $n' > n''$. Time-reversal symmetry mandates the Kramers degeneracy $\varepsilon_{\nu,\sigma}^{(n')} = \varepsilon_{-\nu,-\sigma}^{(n')}$. See Appendix B for more mathematical details.

The full single-electron subband dispersions can be found from solving the eigenvalue problem

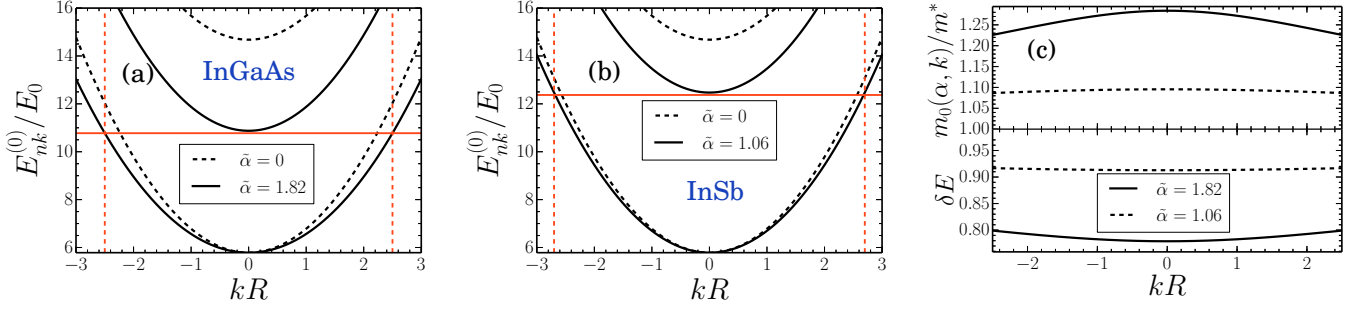


FIG. 1. Electronic structure of noninteracting electrons in nanowires with spin splitting induced by a radial electric field. The solid curves in panel (a) [(b)] show the single-particle energy dispersions of the lowest two subbands obtained for a value of $\tilde{\alpha}$ corresponding to a recent experimental realization using InGaAs [InSb] as the wire material. To illustrate the effect of spin splitting, the corresponding dispersions for $\tilde{\alpha} = 0$ are also plotted as dashed curves. Vertical lines are used to indicate the range of wave numbers for which only the lowest subband is occupied. Panel (c) illustrates more quantitatively the effect of spin-orbit coupling on the lowest nanowire-subband dispersions. In the upper (lower) panel, the ratio of the density-of-states effective masses (subband energies where $\delta E \equiv [E_k^{(0)}(\alpha) - E_0^{(0)}(\alpha)]/[E_k^{(0)}(0) - E_0^{(0)}(0)]$ for finite and for zero $\tilde{\alpha}$ are plotted as a function of wave number.

$$\begin{pmatrix} \varepsilon_{\nu,+}^{(1)} + \kappa^2 & -i\tilde{\alpha}\kappa I_{\nu}^{(11)} & \dots & 0 & -i\tilde{\alpha}\kappa I_{\nu}^{(1n')} & \dots \\ i\tilde{\alpha}\kappa [I_{\nu}^{(11)}]^* & \varepsilon_{\nu,-}^{(1)} + \kappa^2 & \dots & i\tilde{\alpha}\kappa [I_{\nu}^{(1n')}]^* & 0 & \dots \\ \vdots & \vdots & \ddots & \vdots & \vdots & \ddots \\ 0 & -i\tilde{\alpha}\kappa I_{\nu}^{(1n')} & \dots & \varepsilon_{\nu,+}^{(n')} + \kappa^2 & -i\tilde{\alpha}\kappa I_{\nu}^{(n'n')} & \dots \\ i\tilde{\alpha}\kappa [I_{\nu}^{(1n')}]^* & 0 & \dots & i\tilde{\alpha}\kappa [I_{\nu}^{(n'n')}]^* & \varepsilon_{\nu,-}^{(n')} + \kappa^2 & \dots \\ \vdots & \vdots & \ddots & \vdots & \vdots & \ddots \end{pmatrix} \begin{pmatrix} c_{\nu,\kappa}^{(1\uparrow)} \\ c_{\nu,\kappa}^{(1\downarrow)} \\ \vdots \\ c_{\nu,\kappa}^{(n'\uparrow)} \\ c_{\nu,\kappa}^{(n'\downarrow)} \\ \vdots \end{pmatrix} = \varepsilon_{\nu}(\kappa) \begin{pmatrix} c_{\nu,\kappa}^{(1\uparrow)} \\ c_{\nu,\kappa}^{(1\downarrow)} \\ \vdots \\ c_{\nu,\kappa}^{(n'\uparrow)} \\ c_{\nu,\kappa}^{(n'\downarrow)} \\ \vdots \end{pmatrix}, \quad (8a)$$

with matrix elements

$$I_{\nu}^{(nn')} = 2\pi \int_0^1 d\rho \rho \left[\mathcal{F}_{\nu-\frac{1}{2}}^{(\varepsilon_{\nu,+}^{(n)})}(\rho) \right]^* \mathcal{F}_{-\nu-\frac{1}{2}}^{(\varepsilon_{\nu,-}^{(n')})}(\rho). \quad (8b)$$

For the purpose of this study, we only need to obtain the dispersion of the lowest nanowire subband. We find that, for realistic values of $\tilde{\alpha}$ (see for instance the examples below), truncation of the eigenvalue problem (8a) to the subspace spanned by the states $\{|1/2, \uparrow, 1\rangle, |1/2, \downarrow, 1\rangle\}$ and its time-reversed counterpart yields sufficiently accurate results. Hence, in the following, we will use the wave functions

$$\psi_1(r, \varphi, z) = \frac{e^{ikz}}{\sqrt{LR}} \left(-i \sin \eta_{kR} |1/2, \uparrow, 1\rangle + e^{i\varphi} \cos \eta_{kR} |1/2, \downarrow, 1\rangle \right), \quad (9a)$$

$$\psi_2(r, \varphi, z) = \frac{e^{ikz}}{\sqrt{LR}} \left(-i \sin \eta_{kR} |-1/2, \downarrow, 1\rangle + e^{-i\varphi} \cos \eta_{kR} |-1/2, \uparrow, 1\rangle \right) \quad (9b)$$

to describe lowest-subband states with the dispersion

$$E_{1k}^{(0)} \equiv E_{2k}^{(0)} = E_0 \left[(kR)^2 + \frac{1}{2} \left(\varepsilon_{1/2,+}^{(1)} + \varepsilon_{1/2,-}^{(1)} \right) - \frac{1}{2} \sqrt{\left(\varepsilon_{1/2,+}^{(1)} - \varepsilon_{1/2,-}^{(1)} \right)^2 + \left(2\tilde{\alpha}kR I_{1/2}^{(11)} \right)^2} \right]. \quad (10)$$

The coefficients entering Eqs. (9) are

$$\sin \eta_{\kappa} = \frac{1}{\sqrt{2}} \left(1 + \frac{\left| \varepsilon_{1/2,+}^{(1)} - \varepsilon_{1/2,-}^{(1)} \right|}{\sqrt{\left(\varepsilon_{1/2,+}^{(1)} - \varepsilon_{1/2,-}^{(1)} \right)^2 + \left(2\tilde{\alpha}\kappa I_{1/2}^{(11)} \right)^2}} \right)^{\frac{1}{2}}, \quad (11a)$$

$$\cos \eta_{\kappa} = \frac{1}{\sqrt{2}} \left(1 - \frac{\left| \varepsilon_{1/2,+}^{(1)} - \varepsilon_{1/2,-}^{(1)} \right|}{\sqrt{\left(\varepsilon_{1/2,+}^{(1)} - \varepsilon_{1/2,-}^{(1)} \right)^2 + \left(2\tilde{\alpha}\kappa I_{1/2}^{(11)} \right)^2}} \right)^{\frac{1}{2}}, \quad (11b)$$

Figure 1 illustrates the noninteracting-electron band structure of nanowires using parameters relevant to recent experimental realizations³⁴ in Ref. 35 (InGaAs material with conduction-band effective mass $m^* = 0.037m_0$, where m_0 is the electron mass in vacuum, $R = 300$ nm, and $\alpha \mathcal{E} = 10^{-11}$ eV m), and Ref. 36 (InSb, $m^* = 0.013m_0$, $R = 50$ nm, $\alpha \mathcal{E} = 10^{-10}$ eV m). Within our model, the relevant quantity determining the effect

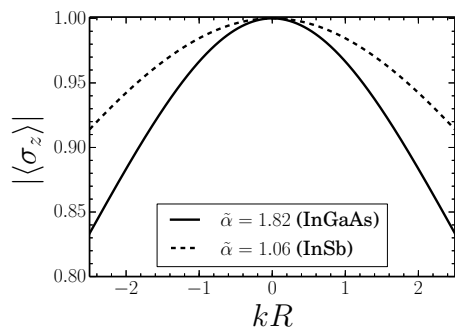


FIG. 2. The magnitude of the expectation value for spin projection parallel to the wire axis, $|\langle\sigma_z\rangle| = \langle\sigma_z\rangle_1 = -\langle\sigma_z\rangle_2 \equiv 2 \sin^2 \eta_{kR} - 1$, for states from the lowest doubly degenerate ($n = 1$ and 2) subband.

of spin-orbit coupling is $\tilde{\alpha}$, which is equal to 1.82 and 1.06 for the InGaAs and InSb nanowires, respectively. For comparison, we show also the result for $\tilde{\alpha} = 0$. As the lowest subband-edge states have quantum numbers $\{\nu = 1/2, \uparrow\}$ and $\{\nu = -1/2, \downarrow\}$, respectively, their energy is independent of $\tilde{\alpha}$, and the spin-orbit coupling only affects the dispersion at finite k . In panel (c), the upper plot shows the ratio of the single-particle density-of-states effective mass,

$$m_0(\alpha, k) = \frac{\hbar^2 k}{\partial E_{1k}^{(0)}/\partial k}, \quad (12)$$

of the lowest subband with and without spin-orbit coupling for the two values of $\tilde{\alpha}$. The lower panel in panel (c) illustrates the relative change in energy for the lowest-subband states due to the spin-orbit coupling. As can be seen from the plot, the renormalization of the single-particle effective mass due to spin-orbit coupling can amount to up to 30% (for $\tilde{\alpha} = 1.82$) and also depends appreciably on the value of the wave vector. In Fig. 2, we show the magnitude of the expectation value of the spin projection along the wire axis for the lowest subband as a function of the wave number k . It decreases with increasing k , as the states given in Eqs. (9) together with (11) become superpositions of \uparrow and \downarrow states for

TABLE I. Properties of the three lowest doubly degenerate nanowire subband edges obtained for parameters applicable to recent experimental realizations.

subband index n	$E_{n0}^{(0)}/E_0$ for $\tilde{\alpha} = 1.82$	$E_{n0}^{(0)}/E_0$ for $\tilde{\alpha} = 1.06$	subband-edge (basis) state
1	5.783	5.783	$ \frac{1}{2}, \uparrow, 1\rangle$
2	5.783	5.783	$ \frac{1}{2}, \downarrow, 1\rangle$
3	10.87	12.47	$ \frac{3}{2}, \uparrow, 1\rangle$
4	10.87	12.47	$ \frac{3}{2}, \downarrow, 1\rangle$
5	18.35	16.85	$ \frac{5}{2}, \uparrow, 1\rangle$
6	18.35	16.85	$ \frac{5}{2}, \downarrow, 1\rangle$

finite k . Table I summarizes properties of the three lowest doubly degenerate subband edges in the two material systems. Note the rather large energy splitting of the (doubly degenerate) next-to-lowest subbands due to the spin-orbit coupling. Without spin-orbit coupling ($\tilde{\alpha} = 0$) the band edge energy of the subbands $n = 3, \dots, 6$ is $E_{n0}^{(0)}/E_0 \approx 14.68$.

III. EFFECT OF SPIN-ORBIT COUPLING ON THE COULOMB-EXCHANGE ENERGY

The Coulomb exchange interaction between electrons renormalizes the quasiparticle dispersion of nanowire subbands, which is then given by¹

$$E_{nk}^{(\text{int})} = E_{nk}^{(0)} + \Sigma_{nk}^{(X)} \quad (13)$$

in terms of the non-interacting subband energy dispersion $E_{nk}^{(0)}$ obtained in the previous Section and the exchange (Fock) self-energy

$$\Sigma_{nk}^{(X)} = - \sum_{n'} \int \frac{dk'}{2\pi} V_{kk'}^{(nn')} n_F(E_{n'k'}) . \quad (14)$$

Here $n_F(E)$ denotes the Fermi-Dirac distribution function, and $V_{kk'}^{(nn')}$ is the matrix element of Coulomb interaction between nanowire-electron states given by

$$V_{kk'}^{(nn')} = C \int d^2 r_{\perp} \int d^2 r'_{\perp} \int_{-L/2}^{L/2} dz \frac{e^{i(k'-k)z}}{\sqrt{z^2 + |\mathbf{r}_{\perp} - \mathbf{r}'_{\perp}|^2}} \times \xi_{n'k'}^{\dagger}(\mathbf{r}_{\perp}) \xi_{nk}(\mathbf{r}_{\perp}) \xi_{nk}^{\dagger}(\mathbf{r}'_{\perp}) \xi_{n'k'}(\mathbf{r}'_{\perp}), \quad (15)$$

where $C \equiv e^2/(4\pi\epsilon_0\epsilon_r)$ is the Coulomb-interaction strength, $\mathbf{r}_{\perp} \equiv (r, \varphi)$ denotes the position vector in the coordinates perpendicular to the wire axis, and $\xi_{nk}(\mathbf{r}_{\perp}) \equiv e^{i\nu\varphi} e^{-i\frac{\sigma_z}{2}\varphi} \phi_{\nu,k}(r)$ is the transverse spinor part of the wavefunction in Eq. (4). In the following, we consider the zero-temperature limit and thus replace the Fermi-Dirac distribution function by $n_F(E) \equiv \Theta(E_F - E)$, with $\Theta(E)$ being the Heaviside step function and E_F denoting the Fermi energy. The condition $E_{nk} \equiv E_F$ defines the Fermi wave vectors k_{Fn} for occupied nanowire subbands. We now focus on the low-density situation where only states in the lowest doubly degenerate subband are occupied up to the Fermi wave vector $k_F = k_{F1} \equiv k_{F2}$. For this situation, we can write

$$\Sigma_{nk}^{(X)} = \frac{-2C}{R} \left[\tilde{\Lambda}_{\text{intra}}(\tilde{\alpha}, \kappa_F, \kappa) + \tilde{\Lambda}_{\text{inter}}(\tilde{\alpha}, \kappa_F, \kappa) \right], \quad (16a)$$

where $\tilde{\Lambda}_{\text{intra}}$ ($\tilde{\Lambda}_{\text{inter}}$) includes contributions arising from the exchange interaction between particles from the same band (from different bands). In the limit $L \rightarrow \infty$, we obtain the explicit expressions

$$\begin{aligned} \tilde{\Lambda}_{\text{intra}}(\tilde{\alpha}, \kappa_{\text{F}}, \kappa) &= \int_{-\kappa_{\text{F}}}^{\kappa_{\text{F}}} d\kappa' \int_0^1 d\varrho \varrho \int_0^1 d\varrho' \varrho' \int_0^{2\pi} d\tilde{\varphi} K_0 \left(|\kappa - \kappa'| \sqrt{\varrho^2 + \varrho'^2 - 2\varrho\varrho' \cos \tilde{\varphi}} \right) \\ &\times \left[\sin^2 \eta_{\kappa} \sin^2 \eta_{\kappa'} \left| \mathcal{F}_0^{(\varepsilon_{1/2,+}^{(1)})}(\varrho) \right|^2 \left| \mathcal{F}_0^{(\varepsilon_{1/2,+}^{(1)})}(\varrho') \right|^2 + \cos^2 \eta_{\kappa} \cos^2 \eta_{\kappa'} \left| \mathcal{F}_{-1}^{(\varepsilon_{1/2,-}^{(1)})}(\varrho) \right|^2 \left| \mathcal{F}_{-1}^{(\varepsilon_{1/2,-}^{(1)})}(\varrho') \right|^2 \right. \\ &\left. + \sin \alpha_{\kappa} \cos \alpha_{\kappa} \sin \alpha_{\kappa'} \cos \alpha_{\kappa'} \left(\left| \mathcal{F}_0^{(\varepsilon_{1/2,+}^{(1)})}(\varrho) \right|^2 \left| \mathcal{F}_{-1}^{(\varepsilon_{1/2,-}^{(1)})}(\varrho') \right|^2 + \left| \mathcal{F}_0^{(\varepsilon_{1/2,+}^{(1)})}(\varrho') \right|^2 \left| \mathcal{F}_{-1}^{(\varepsilon_{1/2,-}^{(1)})}(\varrho) \right|^2 \right) \right], \quad (16b) \end{aligned}$$

$$\begin{aligned} \tilde{\Lambda}_{\text{inter}}(\tilde{\alpha}, \kappa_{\text{F}}, \kappa) &= \int_{-\kappa_{\text{F}}}^{\kappa_{\text{F}}} d\kappa' \sin^2(\eta_{\kappa} - \eta_{\kappa'}) \int_0^1 d\varrho \varrho \int_0^1 d\varrho' \varrho' \int_0^{2\pi} d\tilde{\varphi} \cos \tilde{\varphi} \\ &\times K_0 \left(|\kappa - \kappa'| \sqrt{\varrho^2 + \varrho'^2 - 2\varrho\varrho' \cos \tilde{\varphi}} \right) \mathcal{F}_0^{(\varepsilon_{1/2,+}^{(1)})}(\varrho) \mathcal{F}_{-1}^{(\varepsilon_{1/2,-}^{(1)})}(\varrho) \mathcal{F}_0^{(\varepsilon_{1/2,+}^{(1)})}(\varrho') \mathcal{F}_{-1}^{(\varepsilon_{1/2,-}^{(1)})}(\varrho'), \quad (16c) \end{aligned}$$

where K_0 is the modified Bessel function of the second kind.³⁷ For the numerical evaluation of the intra-band contribution (16b), we employ a modified quadrature method,³⁸ described in greater detail in Appendix C, to deal with the logarithmic singularity encountered when the argument of $K_0(\cdot)$ approaches zero.

The exchange-renormalized density-of-states (quasi-particle) effective mass for the lowest subband can be calculated from

$$m_{\text{int}}(\alpha, k) = \frac{\hbar^2 k}{\frac{\partial E_{1k}^{(0)}}{\partial k} + \frac{\partial \Sigma_{1k}^{(0)}}{\partial k}}. \quad (17)$$

In Fig. 3, we compare the suppression of the quasiparticle effective mass due to the exchange interaction in a nanowire with finite spin-orbit coupling with that of an identical nanowire having zero spin-orbit coupling. As can be seen, the presence of spin-orbit coupling further suppresses the exchange-related quasiparticle-mass by

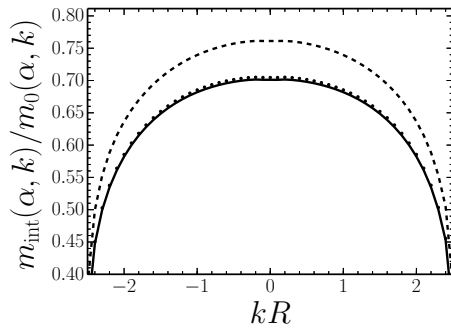


FIG. 3. The ratio of the exchange-renormalized effective quasiparticle mass $m_{\text{int}}(\alpha, k)$ to the bare single-particle effective mass $m_0(\alpha, k)$ is plotted as a function of wave vector k for states from the lowest nanowire subband assuming a material with dielectric constant $\varepsilon_r = 12.9$, $k_{\text{F}}R = 2.5$, and spin-orbit-coupling strength $\tilde{\alpha} = 1.82$ ($\tilde{\alpha} = 0$) as the solid (dashed) curve. For comparison, the dotted curve shows the result obtained under the assumption that the electric field strength varies linearly with the radial coordinate near the wire's center, as described in Appendix A.

10-15% for the parameters used in our calculation. Note also the strong wave-vector dependence of the exchange-renormalized quasiparticle effective mass.

The total exchange energy per particle for the nanowire-electron system is given by¹

$$\frac{E_{\text{X}}}{N} = \frac{1}{2\rho} \sum_n \int \frac{dk}{2\pi} \Sigma_{nk}^{(\text{X})} n_{\text{F}}(E_{nk}), \quad (18)$$

where $\rho = N/L$ is the quasi-1D electron density. Again we focus on the low-density situation where only states in the lowest doubly degenerate subband are occupied up to the Fermi wave vector. For this situation, we can write

$$\frac{E_{\text{X}}}{N} = -\frac{C}{2R} [\Lambda_{\text{intra}}(\tilde{\alpha}, \kappa_{\text{F}}) + \Lambda_{\text{inter}}(\tilde{\alpha}, \kappa_{\text{F}})], \quad (19)$$

where $\Lambda_{\text{intra}}(\tilde{\alpha}, \kappa_{\text{F}}) = \kappa_{\text{F}}^{-1} \int_{-\kappa_{\text{F}}}^{\kappa_{\text{F}}} d\kappa \tilde{\Lambda}_{\text{intra}}(\tilde{\alpha}, \kappa_{\text{F}}, \kappa)$, and the analogous expression applies for Λ_{inter} . Figure 4 illustrates the functional dependences and relative magnitudes of Λ_{intra} and Λ_{inter} . As can be seen, the intra-band contribution is generally dominant and weakly dependent on $\tilde{\alpha}$ values considered here. In contrast, the inter-band contribution changes significantly as a function of $\tilde{\alpha}$.

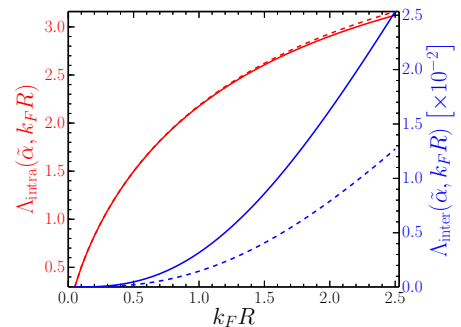


FIG. 4. Scaling functions Λ_{intra} and Λ_{inter} associated with the intra-band and inter-band contributions to the exchange energy per particle in cylindrical nanowires with spin-orbit coupling (note the scale of 10^{-2} for the inter-band contribution). Dashed (solid) curves corresponds to $\tilde{\alpha} = 1.06$ (1.82).

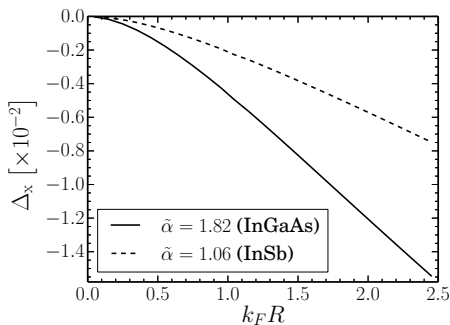


FIG. 5. Relative change Δ_X in the magnitude of the exchange energy resulting from a finite Rashba-type spin-orbit coupling quantified by parameter $\tilde{\alpha}$, as defined in Eq. (20). Note the scale factor of 10^{-2} for the abscissa. The dashed (solid) curve shows the result obtained for $\tilde{\alpha} = 1.06$ (1.82), which corresponds to a recent experimental realization using InSb (InGaAs) as the wire material.

For quantum wires without spin splitting, i.e., in the case $\tilde{\alpha} = 0$, the exchange energy per particle was found to obey a universal scaling form.^{3,39,40} Our expression for E_X/N given in Eq. (19) generalizes these previous results to the case where spin-orbit coupling is finite. The change in magnitude of the exchange energy arising from finite $\tilde{\alpha}$ can be quantified through the relative difference

$$\Delta_X = \frac{E_X(\tilde{\alpha} \neq 0)}{E_X(\tilde{\alpha} = 0)} - 1, \quad (20)$$

which is visualized in Fig. 5. For the values of $\tilde{\alpha}$ that correspond to recent experimental realizations using InGaAs³⁵ and InSb,³⁶ the associated change amounts to a *suppression* of the exchange-energy magnitude which can be up to 1.6%. This behavior is markedly different from the case of a 2D electron system where Rashba spin splitting has been shown²⁰ to result in an *increase* of the exchange energy that is roughly one order of magnitude smaller. Thus the Rashba-type spin-orbit coupling due to a radial electric field in a cylindrical nanowire system is more similar to a 2D hole system where the interplay between quantum confinement and spin-orbit effects also results in a suppression of the exchange energy.¹⁸

IV. CONCLUSIONS

We have studied theoretically the electronic properties of the quasi-1D electron system realized in a cylindrical quantum wire subject to a radially symmetric Rashba-type spin-orbit coupling. We determined the single-particle states for a hard-wall confinement using subband $\mathbf{k} \cdot \mathbf{p}$ theory. Focusing on the situation where only the lowest quasi-1D subband is occupied, we observed that the corresponding energy dispersion can be very accurately (to within 0.5% error) calculated from an effective 2×2 Hamiltonian. Taking the material parameters of two

experimentally studied nanowire systems (one based on InGaAs and the other on InSb) as input, we have determined the influence of the spin-orbit strength on the lowest quasi-1D subband's energy dispersion and on the spin projection of its corresponding eigenstates parallel to the wire axis, finding both quantities to be affected by tens of percent due to the presence of spin-orbit coupling. In particular, the density-of-states effective mass of the noninteracting system turns out to be increased by 20-25% for parameters applicable to the InSb nanowires.

With single-particle states in hand, we calculated the quasiparticle effective mass for the lowest subband and found its exchange-related suppression to be significantly larger in magnitude (by 10-15% for parameters used in our calculations) when spin-orbit coupling is finite. In contrast, the magnitude of the exchange energy per particle is marginally reduced (by upto 1.6%) by spin-orbit coupling effects. Thus we find that any meaningful discussion of the interplay between spin-orbit coupling and exchange interactions in quantum wires needs to be carefully focused on specific physical quantities, as their relevant parametric dependences can be quite different, both qualitatively and quantitatively. Furthermore, often the relevance of interaction effects in an electron system is quantified in relative terms by a parameter r_s that is related to the ratio of contributions to the total energy arising from interactions and the single-electron dispersion, respectively.¹ In the present context, spin splitting causes an increase in the single-particle effective mass of quasi-1D electrons simultaneously with the suppression of the exchange energy. As the relative change in the increase in noninteracting system's effective mass is an order of magnitude larger than the relative decrease of the exchange energy, the relative importance of interactions as measured by r_s turns out to be enhanced by spin-orbit coupling.⁴¹

While we have focused on a specific configuration of confinement and spin-orbit coupling, our general results and overall conclusions can be expected to apply also to other spin-orbit-coupled nanowire systems, e.g., the one considered in Ref. 42.

ACKNOWLEDGMENTS

We gratefully acknowledge useful discussions with S. Chesi.

Appendix A: Radial electric-field profile

A proper self-consistent treatment of electrostatic effects generally requires the application of an iterative Schrödinger-Poisson solver method that is specifically adapted to the sample layout. An added complication arises from the intricate way how the Rashba spin-orbit coupling strength needs to be determined from expectation values of the electric field taken in a multi-band

bound state.⁵ As we intend to focus on the broad implications of spin-orbit coupling in confined systems, we decided to make an assumption about the radial profile of the electric field entering in the spin-orbit term that enables us to obtain rather general physical insights. Here

$$2\pi r L \mathcal{E}(r) = \frac{-e}{\varepsilon_0 \varepsilon_r} \sum_j \sum_{|k| \leq k_F} \int_0^L dz \int_0^{2\pi} d\varphi \int_0^r dr' r' [\psi_j(r', \varphi, z)]^\dagger \psi_j(r', \varphi, z) \quad , \quad (\text{A1})$$

with the single-particle wave functions $\psi_{1,2}(r, \varphi, z)$ given in Eq. (9). Straightforward calculation yields $\mathcal{E}(r) = \mathcal{E}_0 [S_{k_F R} \mathcal{P}_0(r/R) + C_{k_F R} \mathcal{P}_1(r/R)]$, where $\mathcal{E}_0 = -Ne/(2\pi RL \varepsilon_0 \varepsilon_r)$ is an overall scale containing the number of particles N , $S_\kappa = \frac{1}{\kappa} \int_0^\kappa d\kappa' \sin^2 \eta_{\kappa'}$ and $C_\kappa = \frac{1}{\kappa} \int_0^\kappa d\kappa' \cos^2 \eta_{\kappa'}$ are weightings of the mixed bound-state contributions for the lowest nanowire subband, and

$$\mathcal{P}_{0(1)}(\varrho) = \frac{2\pi}{\varrho} \int_0^\varrho d\varrho' \varrho' \left[\mathcal{F}_{0(1)}^{(\varepsilon_1^{(1)/2, +(-)})}(\varrho') \right]^2 \quad (\text{A2})$$

are the radial density profiles associated with the relevant bound states.

The calculated full electric-field profile is shown in Fig. 6. Our results from the main paper suggest that generally $S_{k_F R} \approx 1$, $C_{k_F R} \approx 0$; hence $\mathcal{E}(r)$ should be essentially determined by the $\mathcal{P}_0(r/R)$ contribution. This is indeed observed in the numerical evaluation. Also, as expected from the shape of the density profile associated with the $m = 0$ bound-state wave function (cf. Appendix B), the leading behaviour at $r/R \ll 1$ is linear.

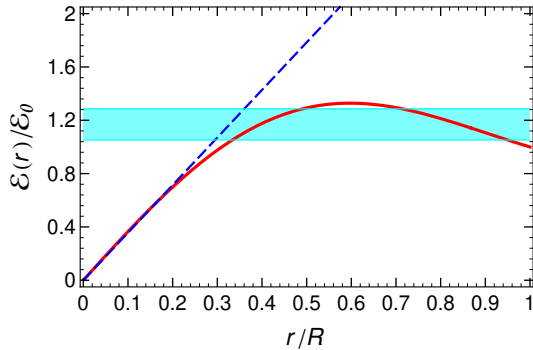


FIG. 6. The radial profile of the electric-field magnitude $\mathcal{E}(r)$ associated with our calculated nanowire states is plotted as the solid red curve. The asymptotically linear behaviour for small r/R is captured by the blue dashed line. The horizontal (cyan) band indicates the range of field values that lie within 10% of the mean value. The weak variation of $\mathcal{E}(r)$ for $r \gtrsim 0.3R$ motivates our assumption of a constant field magnitude for the radially symmetric Rashba term in Eq. (2). The scale of the electric field is $e\mathcal{E}_0 = 1.6\kappa_F \mu\text{eVnm}^{-1}$ for the scenario based on InGaAs while it is $e\mathcal{E}_0 = 41\kappa_F \mu\text{eVnm}^{-1}$ for InSb.

we show the basic consistency of this assumption with the electrostatics of the bound-state configuration for our system.

Application of Gauss's law using the cylindrical symmetry of the nanowire geometry yields the relation

However, over most of the wire's cross-section, the field profile is quite well approximated by a constant, which supports our pragmatic assumption. It is also observed from direct calculation that $S_{k_F R}$ and $C_{k_F R}$ are almost constant in the relevant range $k_F R < 2.5$ where only the lowest nanowire subband is occupied.

In order to confirm that the omission of the linear electric field dependence for $r/R \lesssim 0.3$ will not alter our conclusions, we consider an electric field which is modelled by a linear dependence on the radial coordinate upto $\varrho < \varrho_0$ and a constant for $\varrho > \varrho_0$. In terms of the dimensionless Hamiltonian description in Eq. (5), this implies the replacement $\tilde{\alpha} \rightarrow \tilde{\alpha} \left[\frac{\varrho}{\varrho_0} \Theta(\varrho_0 - \varrho) + \Theta(\varrho - \varrho_0) \right]$. Proceeding as in the case of a constant electric field, we find for the wave functions in the region with $\varrho < \varrho_0$ the Bessel-function solutions $J_m(\varrho\sqrt{\varepsilon + m\tilde{\alpha}/\varrho_0})$. For the region $\varrho > \varrho_0$, we obtain wave functions which are a superposition of modified Laguerre functions (see Appendix B) and confluent hypergeometric functions of the second kind. Applying the standard matching conditions at $\varrho = \varrho_0$ to ensure continuity of the wave functions and their products with the velocity-operator in the transverse direction determines the unknown coefficients. In this context, it should be noted that the lowest state is independent of the electric field. Considering the scenario with $\tilde{\alpha} = 1.82$ as an example and taking into account the hard-wall boundary condition, we find only small changes for the band-edge energies $E_{(3,4)0}^{(0)}/E_0 = 11.07$ and $E_{(5,6)0}^{(0)}/E_0 = 18.22$ when $\varrho_0 = 0.3$ (cf. Table I). In Fig. 7 we show the real part (dashed curve) and imaginary part (dotted curve) of the subband edge wave function for spin up of the second-excited state $|-1/2, \uparrow, 1\rangle$ and compare this with the corresponding wave function obtained under the assumption of a constant radial electric-field strength. We can therefore conclude that the linear electric field dependence for $\varrho < \varrho_0$ changes the relevant wave functions used in our calculations only slightly. For $\kappa \neq 0$, we find that the matrix element $I_{1/2}^{(11)} \approx -0.884$, while it is $I_{1/2}^{(11)} \approx -0.916$ with the assumption of a constant electric field, yielding only sub-percent changes for the dispersions and exchange-related quantities (see for instance Fig. 3).

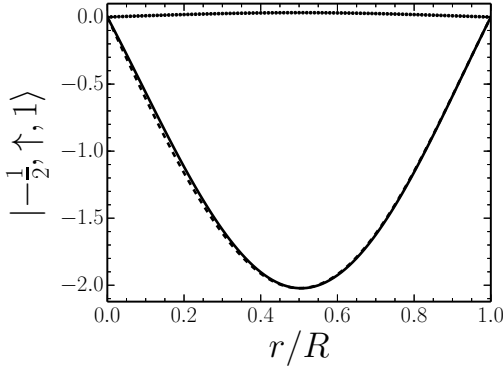


FIG. 7. Real part (dashed curve) and imaginary part (dotted curve) of the subband edge wave function for spin up of the second-excited state obtained for an electric field that depends linearly on the wire's radius upto $\varrho = 0.3$ and is constant for $\varrho > 0.3$. For comparison we show the real wave function of the corresponding state (solid curve) obtained under the assumption of a throughout constant electric field.

Appendix B: Solution of the radial-confinement problem

The general solution of the differential equations present in the diagonal entries of Eq. (5) are power series, given by,

$$\mathcal{F}_m^{(\varepsilon_{\nu,\pm}^{(n')})}(\varrho) = \varrho^m (a_0 + a_1 \varrho + \sum_{n=2}^{\infty} a_n \varrho^n) \quad (\text{B1})$$

which fulfill the relation $\mathcal{F}_{-m}^{(\varepsilon_{\nu,\pm}^{(n')})}(\varrho) = \mathcal{F}_{+m}^{(\varepsilon_{\nu,\mp}^{(n')})}(\varrho)$ yielding the eigenstates. Disregarding the ill-behaved and unphysical part in the expansion at the origin, the coefficients of the polynomials are determined by the recursion relation

$$n(n \pm 2m)a_n + m\tilde{\alpha}a_{n-1} + \varepsilon_{\nu,\pm}^{(n')}a_{n-2} = 0, \quad (\text{B2})$$

with $a_1 = -\tilde{\alpha}m/(1 \pm 2m)a_0$, where the upper (lower) sign applies to $m > 0$ ($m < 0$). The coefficient a_0 is determined by the normalisation condition $2\pi \int_0^1 d\varrho \varrho |\mathcal{F}_m^{(\varepsilon_{\nu,\pm}^{(n')})}(\varrho)|^2 = 1$. We note that the polynomial with coefficients given by Eq. (B2) represents a modified Laguerre function that becomes the standard Bessel function $J_0(\sqrt{\varepsilon_{\nu,\pm}^{(n')}}\varrho)$ for $\tilde{\alpha} = 0$ and/or $m = 0$. The band-edge energies, $\varepsilon_{\nu,\pm}^{(n')}$ are found by imposing hard wall boundary conditions on the radial wave function, i.e. for $r = R$, we require

$$\mathcal{F}_m^{(\varepsilon_{\nu,\pm}^{(n')})}(\varrho = 1) = 0. \quad (\text{B3})$$

For not too large values of $\tilde{\alpha}$, the lowest spin- \uparrow (\downarrow) subband-edge state has $\nu = 1/2$ ($-1/2$) total angular momentum. However, as seen from Fig. 8, a level crossing

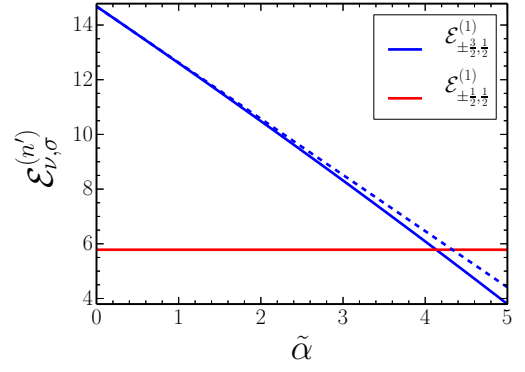


FIG. 8. Energy eigenvalues of the lowest two doubly degenerate quasi-1D subband edges, plotted as a function of the effective Rashba spin-orbit-coupling parameter $\tilde{\alpha}$. The blue dashed curve is an approximation based on Eq. (B4).

occurs for $\tilde{\alpha} \approx 4.2$, beyond which the new lowest spin- \uparrow (\downarrow) subband edge is a state with $\nu = \pm 3/2$ ($-3/2$). The variation of the band-edge energy $\varepsilon_{\pm 3/2,\pm}^{(1)}$ as a function of $\tilde{\alpha}$ can be approximated using standard perturbation theory, yielding

$$\varepsilon_{\pm 3/2,\pm}^{(1)} = \varepsilon_0 - \tilde{\alpha} \frac{\int_0^1 d\varrho J_1^2(\varrho\sqrt{\varepsilon_0})}{\int_0^1 d\varrho \varrho J_1^2(\varrho\sqrt{\varepsilon_0})}, \quad (\text{B4})$$

where $\varepsilon_0 \approx 14.68$ is the band edge energy of the corresponding band for $\tilde{\alpha} = 0$.

Appendix C: Regularisation of the integrand for calculating the exchange energy

In the calculation of the exchange energy we have to deal with integrals of the form

$$\mathcal{I} = \iint dk dk' G(k, k') K_0 \left(|k - k'| \sqrt{r^2 + r'^2 - 2rr' \cos \varphi} \right), \quad (\text{C1})$$

with $G(k, k')$ being a smooth function of k and k' . A logarithmic singularity occurs when the argument of $K_0(\cdot)$ vanishes. This happens when either the square root is zero, at $\vec{r}_\perp = \vec{r}'_\perp$, or when $k = k'$. To regularise the integral for the case where $\vec{r}_\perp = \vec{r}'_\perp$, we add a small amount 0^+ to the term under the square root. Then by decreasing the value of 0^+ , we perform a series of calculations until the result for the exchange energy doesn't change within a certain tolerance.

The situation for $k = k'$ can be regularised analytically. To this end, we add to and subtract from Eq. (C1) the term

$$\iint dk dk' G(k, k) \ln \left(|k - k'| \sqrt{r^2 + r'^2 - 2rr' \cos \varphi + 0^+} \right). \quad (\text{C2})$$

Adding this term to Eq. (C1) cancels the logarithmic

singularity. The k' -integration of the subtracted term can be performed analytically and Eq. (C1) becomes

$$\mathcal{I} = \int dk \left\{ \left[\int dk' G(k, k') K_0 \left(|k - k'| \sqrt{r^2 + r'^2 - 2rr' \cos \varphi} \right) + G(k, k) \ln \left(|k - k'| \sqrt{r^2 + r'^2 - 2rr' \cos \varphi} \right) \right] - G(k, k) \left[k \ln \left(\frac{k_F + k}{k_F - k} \right) - 2k_F + 2k_F \ln \left(\sqrt{k_F^2 - k^2} \sqrt{r^2 + r'^2 - 2rr' \cos \varphi} + 0^+ \right) \right] \right\}. \quad (\text{C3})$$

The expression Eq. (C3) is manifestly finite for $k = k'$.

- * michele.governale@vuw.ac.nz
 † uli.zuelicke@vuw.ac.nz
- ¹ G. Giuliani and G. Vignale, *Quantum Theory of the Electron Liquid* (Cambridge University Press, Cambridge, UK, 2005).
 - ² T. Ando, A. B. Fowler, and F. Stern, *Rev. Mod. Phys.* **54**, 437 (1982).
 - ³ A. Gold and A. Ghazali, *Phys. Rev. B* **41**, 8318 (1990).
 - ⁴ P. Y. Yu and M. Cardona, *Fundamentals of Semiconductors*, 4th ed. (Springer, Berlin, 2010).
 - ⁵ R. Winkler, *Spin-Orbit Coupling Effects in Two-Dimensional Electron and Hole Systems* (Springer, Berlin, 2003).
 - ⁶ R. Winkler, *Phys. Rev. B* **71**, 113307 (2005).
 - ⁷ G. Dresselhaus, *Phys. Rev.* **100**, 580 (1955).
 - ⁸ E. I. Rashba, *Fiz. Tverd. Tela (Leningrad)* **2**, 1224 (1960), [*Sov. Phys. Solid State* **2**, 1109 (1960)].
 - ⁹ Y. A. Bychkov and E. Rashba, *JETP Lett.* **39**, 78 (1984).
 - ¹⁰ M. Combescot and P. Nozières, *J. Phys. C: Solid State Phys.* **5**, 2369 (1972).
 - ¹¹ J. Schliemann, *Phys. Rev. B* **74**, 045214 (2006).
 - ¹² J. Schliemann, *Phys. Rev. B* **84**, 155201 (2011).
 - ¹³ F. V. Kyrychenko and C. A. Ullrich, *Phys. Rev. B* **83**, 205206 (2011).
 - ¹⁴ W. O. G. Schmitt, *Phys. Rev. B* **50**, 15221 (1994).
 - ¹⁵ S.-J. Cheng and R. R. Gerhardts, *Phys. Rev. B* **63**, 035314 (2001).
 - ¹⁶ S. Chesi and G. F. Giuliani, *Phys. Rev. B* **75**, 155305 (2007).
 - ¹⁷ A. Scholz, T. Dollinger, P. Wenk, K. Richter, and J. Schliemann, *Phys. Rev. B* **87**, 085321 (2013).
 - ¹⁸ T. Kernreiter, M. Governale, R. Winkler, and U. Zülicke, *Phys. Rev. B* **88**, 125309 (2013).
 - ¹⁹ M. Pletyukhov and V. Gritsev, *Phys. Rev. B* **74**, 045307 (2006).
 - ²⁰ S. Chesi and G. F. Giuliani, *Phys. Rev. B* **83**, 235308 (2011).
 - ²¹ S. Chesi and G. F. Giuliani, *Phys. Rev. B* **83**, 235309 (2011).
 - ²² A. Agarwal, S. Chesi, T. Jungwirth, J. Sinova, G. Vignale, and M. Polini, *Phys. Rev. B* **83**, 115135 (2011).
 - ²³ W. Häusler, *Phys. Rev. B* **63**, 121310 (2001).
 - ²⁴ V. Gritsev, G. Japaridze, M. Pletyukhov, and D. Baeriswyl, *Phys. Rev. Lett.* **94**, 137207 (2005).
 - ²⁵ A. Schulz, A. De Martino, P. Ingenhoven, and R. Egger, *Phys. Rev. B* **79**, 205432 (2009).
 - ²⁶ F. Maier, T. Meng, and D. Loss, *Phys. Rev. B* **90**, 155437 (2014).
 - ²⁷ T. Giamarchi, *Quantum Physics in One Dimension* (Clarendon Press, Oxford, UK, 2004).
 - ²⁸ J. Alicea, *Rep. Prog. Phys.* **75**, 076501 (2012).
 - ²⁹ J. Klinovaja, P. Stano, and D. Loss, *Phys. Rev. Lett.* **109**, 236801 (2012).
 - ³⁰ K. Storm, G. Nylund, L. Samuelson, and A. P. Micolich, *Nano Lett.* **12**, 1 (2012).
 - ³¹ D. A. Broido and L. J. Sham, *Phys. Rev. B* **31**, 888 (1985).
 - ³² S.-R. E. Yang, D. A. Broido, and L. J. Sham, *Phys. Rev. B* **32**, 6630 (1985).
 - ³³ U. Rössler, *Solid-State Theory: An Introduction*, 2nd ed. (Springer, Berlin, 2009) pp. 128-129.
 - ³⁴ Even though the type of Rashba spin splitting realized in these experiments differs from that adopted in our work, the same bandstructure-related prefactors and orders of magnitude for the electric field apply in both their and our systems. This motivates our use of spin-orbit-coupling strengths measured in Refs. 35 and 36.
 - ³⁵ T. Schäpers, J. Knobbe, and V. A. Guzenko, *Phys. Rev. B* **69**, 235323 (2004).
 - ³⁶ I. van Weperen, B. Tarasinski, D. Eeltink, V. S. Pribiag, S. R. Plissard, E. P. A. M. Bakkers, L. P. Kouwenhoven, and M. Wimmer, preprint arXiv:1412.0877v1.
 - ³⁷ M. Abramowitz and I. A. Stegun, *Handbook of Mathematical Functions* (Dover, New York, 1964).
 - ³⁸ C. Chao and S. Chuang, *Phys. Rev. B* **43**, 6530 (1991).
 - ³⁹ L. Calmels and A. Gold, *Phys. Rev. B* **52**, 10841 (1995).
 - ⁴⁰ L. Calmels and A. Gold, *Phys. Rev. B* **56**, 1762 (1997).
 - ⁴¹ S. Chesi, private communication.
 - ⁴² A. Bringer and T. Schäpers, *Phys. Rev. B* **83**, 115305 (2011).